Fragmentation by thermal relaxation of zirconium oxide aerogel

2000 J. Phys.: Condens. Matter 12 7547

(http://iopscience.iop.org/0953-8984/12/34/302)

J. Phys.: Condens. Matter **12** (2000) 7547–7557. Printed in the UK PII: S0953-8984(00)12464-6

Fragmentation by thermal relaxation of zirconium oxide aerogel

Nathalie Olivi-Tran†, André Lecomte‡, Pascal Lenormand‡ and Alain Dauger‡

† Institut Non Linéaire de Nice, UMR 6618, 1361 route des Lucioles, Sophia-Antipolis, 06560 Valbonne, France

‡ Science des Procédés Céramiques et de Traitements de Surface, UMR 6638, ENSCI, 47 à 73 Avenue Albert Thomas, 87065 Limoges, France

Received 8 March 2000, in final form 18 July 2000

Abstract. Zirconia aerogels are made of connected fractal clusters composed of small crystalline particles. When heated at a low temperature (i.e. 0.13 times the melting temperature), the mass transport process which predominantly occurs is surface diffusion. Due to the local character of surface diffusion, fragmentation appears in the sample during thermal annealing. This particular evolution of the structure is numerically analysed and experimentally studied by small-angle x-ray scattering.

1. Introduction

Aerogels are dry gel networks made by supercritical extraction of the pore liquid from a gel, which exhibit a fractal structure between two characteristic lengths. Indeed an aerogel is made of a framework of connected fractal clusters. The size of the clusters is the upper fractal limit. Each of these clusters is composed of particles. The mean size of these particles represents the lower limit of the fractal domain.

Studies on fragmentation of aerogels are very rare. Up to now, there have only been works on two-dimensional fractal aggregates [1,2]. This shows a different behaviour to silica aerogels when heated. Indeed, the matter transport phenomena which occur are, at low temperature, surface diffusion and evaporation–redeposition [3], and these matter transport phenomena lead generally to fragmentation of the whole of a structure which is heated. We present here a numerical approach to this fragmentation phenomenon and we compare the results to experimental small-angle scattering data on zirconia aerogels.

Experimentally, we investigated the early stage of structural evolution in fractal crystalline matter with small-angle x-ray scattering (SAXS) measurements. The material used is a zirconia (ZrO_2) aerogel prepared by supercritical drying of wet gels made from zirconium *n*-propoxide, acetylacetone, *n*-propanol and water. It has a well established hierarchical structure made of connected mass fractal clusters resulting from the aggregation of small zirconium oxide particles. Moreover, the primary units are crystallized in the tetragonal zirconia form and each particle is a single crystal [4]. The experiments carried out here consist in a thermal treatment at 38 °C, a very low temperature ($0.13T_f$) as compared to the zirconia melting temperature ($T_f = 2700$ °C). In view of the crystalline nature of the material, of the low temperature used

0953-8984/00/347547+11$30.00

and of the very small size of the particles, the expected mass transport mechanism is obviously surface diffusion [3].

In sections 2 and 3, we shall present the experimental method and numerical model necessary to characterize the structure of zirconia aerogels during surface diffusion restructuring. In section 4, results are given. In section 5, a discussion on our results is given which focus on the interpretation of the SAXS intensity curves and on the fragmentation effect. Finally, in section 6, we shall give our conclusions.

2. Experimental procedure

To prepare the zirconia precursor gels, we used the zirconium *n*-propoxide, *n*-propanol, acetylacetone (acacH) and water system [5]. The zirconium *n*-propoxide concentration and the hydrolysis and complexing ratios were $C = [Zr(OC_3H_7)_4] = 0.25$ mol l^{-1}, $W = [H_20]/[Zr(OC_3H_7)_4] = 10$ and $R = [acacH]/[Zr(OC_3H_7)] = 0.7$ respectively. In order to obtain an aerogel, the solvent was evacuated by supercritical drying of the alcogel in an autoclave in presence of *n*-propanol ($T = 270\ ^\circ$C, $P = 5.52$ MPa).

The aerogel was transparent with an initial macroscopic density of 0.22. In the untreated aerogel x-ray diffraction pattern, the Bragg peaks were very broad and showed that the primary units of the structure were crystallized in the zirconia tetragonal form, in agreement with TEM experiments [5].

For time–temperature-dependent investigations, i.e. on surface diffusion restructuring, aerogel slices were directly put in an oven held at 350 °C. The samples were removed for analysis after the desired time intervals.

In order to study the structure of our material, we used an original SAXS experimental set-up with a point collimation geometry. The Cu Kα_1 incident beam was provided by a double channel-cut germanium monochromator adapted to an 18 kW rotating-anode x-ray generator.

The scattered intensity was recorded using a linear position-sensitive detector. Two sample–detector distances (0.5 m and 1.5 m) were successively used to cover a q-range from 0.04 to 4 nm^{-1} where q is the scattering vector $q = 4\pi\lambda^{-1}\sin(\theta)$, λ the wavelength and 2θ the scattering angle. Appropriate corrections for slit scattering, background scattering and absorption effects were applied to the raw data.

We did not use here an absolute scale for the SAXS curves. Absolute scales are mainly used to extract a specific surface or the molecular mass of polymers. In most cases, one is interested in the curve shape and an absolute scale is hence not necessary. For our aerogels, the transmission of the beam remains constant because we have no mass variation and no dimensional shrinking, and the beam intensity always 'sees' the same quantity of matter. The curves at different stages of heat treatment are then directly comparable.

3. Numerical procedure

3.1. Aerogel representation

To generate the aerogel structure, we have considered an on-lattice version of the DLCA (diffusion-limited cluster–cluster aggregation) model in three dimensions, dealing with identical particles in a cubic box [6]. The particles are modelled by small cubes of edge length $2a_0$ always located on the lattice cells of dimension a_0 of a cubic lattice. The particles move inside a box of edge length $2La_0$, with periodic boundary conditions at the box edges,

and their number N is such that the volume fraction c is set to the desired value:

$$c = \frac{Nv}{8L^3a_0^3} \tag{1}$$

where v is the volume of one particle of edge length $2a_0$ (this value of the edge length is valid at time $t = 0$). For convenience, we will take in the following the value $a_0 = 1$. The particles are first randomly distributed in the box using a random sequential addition procedure, avoiding double occupancy of the lattice cells. Then these particles are allowed to undergo random walks on the lattice (jumping to nearest-neighbouring cells at random) and they irreversibly stick when they try to overlap.

Aggregates of particles are also allowed to diffuse together with the individual particles and to stick to other particles or to other aggregates. In this diffusive motion, the aggregates are rigid and their diffusion constant is taken to be proportional to the inverse of their radius of gyration.

When the initial packing fraction c is sufficiently large (larger than a threshold value c_g which tends to zero as the box size tends to infinity [7]), the final aggregate forms a gelling network which extends from edge to edge in the box and can be described by a loose random packing of connected fractal aggregates, of fractal dimension $D = 1.8$, whose mean size ξ decreases as c increases according to the scaling law

$$\xi \propto c^{-1/(3-D)}. \tag{2}$$

3.2. Surface diffusion restructuring modelling

We need here an exact definition of the different kinds of particle that we shall discuss in the following. *Elementary particles* are the cubes of edge length equal to $2a_0 = 2$ used for the construction of the numerical aerogels. This choice of a factor 2 for the edge length is arbitrary and represents a balance between the computer's performance and the fragmentation rate. It does not affect the final result, but the smaller this factor is the more precise the shape of the internal structure is. When these *elementary particles* are divided into smaller pieces, for numerical calculation purposes, one obtains *subparticles*. For experimental aerogel, this term *elementary particles* retains the meaning commonly accepted. During the experimental or numerical surface diffusion restructuring, these *elementary particles* will grow and become particles. Finally we call the constituents of the numerical or experimental aerogel below which scale the sample is no longer fractal *particles*: these *particles* are dense and may be constituted by the merging of *elementary particles* or *subparticles* and no assumption regarding the particle form is made. At time $t = 0$ (i.e. before restructuring has begun), *particles* and *elementary particles* are the same.

We use here a Monte Carlo algorithm. Our method is similar to that employed, in two dimensions, by Irisawa *et al* [2], but it is adapted to a three-dimensional cubic lattice. We start with a numerical aerogel built as described in the previous section, i.e. on-lattice DLCA aggregates in a cubic box with periodic boundary conditions. Each elementary particle of this DLCA aerogel has an edge length equal to 2. This allows us to cut each elementary particle into eight subparticles which have this time an edge length equal to 1 (remember that we took $a_0 = 1$). If we did not do this, the initial aggregate would break into pieces almost immediately because for most parts of this fractal cluster the connection is by a single particle.

Each subparticle has a probability P of moving from its site on the lattice to an unoccupied nearest-neighbouring site. This probability depends on the bonding energy of each subparticle, i.e. on the number N_i of neighbours of the site occupied by the subparticle and on the number N_f of neighbours of the unoccupied site, as follows:

$$P = \exp[-A(N_i - N_f)] \tag{3}$$

where $A = E_b/kT$ with E_b the energy per neighbour, k the Boltzmann constant and T the temperature. In the particular case where $N_f = 0$ (corresponding to the subparticle 'melting', i.e. undergoing a movement toward a site with no neighbour), the probability is

$$P = \exp[-AN_i - B] \tag{4}$$

where $B = \Delta\mu/kT$ with $\Delta\mu$ the chemical potential gain associated with solidification (i.e. $-\Delta\mu$ is the chemical potential associated with melting). B corresponds to evaporation–condensation. Indeed, to leave the surface, a subparticle has to overcome a potential barrier which is created by the bulk: the chemical potential corresponds to the energy of the bonding of the melting subparticle to the bulk. For subparticles remaining on the aerogel structure, the chemical potential is the same everywhere, so there is no difference between the chemical potential at one site in the bulk and that at another site in the bulk, and hence the chemical potential does not appear in the probabilities of moving for subparticles remaining on the aerogel structure.

So, finally, at each Monte Carlo step the probabilities of moving for each subparticle are computed and one move is chosen at random according to these probabilities.

3.3. Small-angle scattering intensity calculation

From single-scattering theory, the small-angle scattering intensity $I(\boldsymbol{q})$, where $\boldsymbol{q}$ is the scattering wave vector, is proportional to the square of the Fourier transform of the density distribution in direct space [8, 9]. We introduce a density function $\delta(\boldsymbol{r})$ which is defined as equal to 1 if the site centred at $\boldsymbol{r}$ is occupied by a subparticle and equal to 0 if not. Therefore, the intensity shows the following proportionality:

$$I(q) \propto \left| \sum_{\boldsymbol{r}} \delta(\boldsymbol{r}) \exp \mathrm{i}\boldsymbol{q} \cdot \boldsymbol{r} \right|^2. \tag{5}$$

As usual, we introduce a double sum to expand the square and, assuming isotropy, we average over all the directions of $\boldsymbol{q}$ to get

$$I(q) \propto \sum_{\boldsymbol{r}_1} \sum_{\boldsymbol{r}_2} \delta(\boldsymbol{r}_1)\delta(\boldsymbol{r}_2) \frac{\sin qr}{qr} \tag{6}$$

where

$$r = |\boldsymbol{r}_1 - \boldsymbol{r}_2|. \tag{7}$$

Then transforming the double sum into a sum over the possible values for the distance r and separating the $r = 0$ contribution from the others, we get

$$I(q) \propto \left(1 + \sum_{r \neq 0} F_a(r)\right) \frac{\sin qr}{qr} \tag{8}$$

where $F_a(r)$ is the mean number of subparticles at a distance r from a given subparticle (the on-lattice pair correlation function).

One has to note that formula (8) is an approximation to the real intensity curve $I(q)$; the smaller the subparticles, the better our approximation as noted previously in reference [10]. We are interested here in the evolution of the fractal regime in the SAXS curve. Since this fractal regime is the same in structure as the total intensity [10], our computation can be applied to our analysis of the aerogel structure.

One should remark that in the numerical calculations of the intensity, due to the Fourier transform, the value of q is equivalent to $2\pi/l$ where l is the corresponding length scale.

4. Experimental and numerical results

We first present the experimental results for the small-angle scattering intensity. The raw aerogel SAXS curve shows a broad scattered intensity maximum at $q_m = 0.05$ nm^{-1}, an intermediate power-law behaviour running over one decade in q with a slope of -2.3 and a crossover between the fractal and the Porod regimes at about 2.6 nm^{-1}. So, ZrO_2 aerogel has a well established structure made up of connected mass fractal clusters, with a size around 120 nm and an apparent fractal dimension of 2.3. These clusters result from aggregation of small zirconium oxide particles with a high degree of crystallinity in the tetragonal zirconia form. The sizes of these primary units determined by small-angle x-ray scattering and x-ray diffraction are the same and about 2.5 nm. Each particle is a single crystal [3, 4].

Figure 1(a) represents the SAXS intensity for the experimental part of this work. The intensity curves are plotted for several isothermal annealing durations ranging from 0.5 h to 231 h at 350 °C. Figure 1(b) represents also the small-angle scattering intensity, but this time for the numerical part of our work. The following values of the parameters of the simulation have been chosen: $A = 20$, $B = 30$, and the simulation box size was taken to be 100. The value of A does not affect the final structure of the aerogel but only the duration of the evolution. Meanwhile, the value of B affects the number of isolated particles in the final sample: it represents a chemical potential value. In all of the following, the second stage of thermal annealing was taken to be after 6×10^3 Monte Carlo steps and the nearly final stage to be at 10^8 Monte Carlo steps.

The three intensity curves represent the three stages of thermal annealing, i.e. the three different Monte Carlo durations of annealing. The small oscillations in the curves arise from the discrete state of the subparticle positions. As can be seen, the intensities in the low-q portions of the experimental and numerical SAXS curves do not change significantly, but the intermediate- and large-q regions are appreciably modified. The extent of the fractal regime is gradually reduced and vanishes and the Porod regime grows towards lower q-values. Simultaneously, the intensity distribution in the intermediate region is significantly modified since the scattered intensity increases whereas it decreases at higher q-values. A crossover results from these two opposing behaviours and a narrow region of almost constant intensity clearly appears around $q_{crossover} = 1$ nm^{-1}, i.e. $l_{crossover} = 2\pi a_0$.

One can remark that in figure 1(a) as well as in figure 1(b) the experimental curves and the numerical ones immediately below the crossover show a sigmoidal shape. This sigmoidal shape comes from the Rayleigh scattering of uniformly size-distributed particles, as we have obtained numerically and certainly experimentally. For more details on this kind of small-angle scattering behaviour, see [11, 12].

Figures 2(a) and 2(b) present a part of a simulation box for two stages of thermal annealing: the initial stage and a stage near the end of the process, where there is almost no further evolution in the internal structure. We have to add that the single subparticles which are disconnected from the whole structure have a small Monte Carlo probability of moving, so their diffusion is very slow. Hence the very final stage would be a group of large fragments with no single disconnected subparticles. Unhappily, the computation time required to obtain this stage would be too long, but the final results (such as the crossover and the sigmoidal shape of the small-angle scattering curves) would not change. It is obvious that there is a fragmentation process. There are several fragments which are no longer connected to the rest of the structure. Remark that the different fragments do not fall apart: we did not add gravitation in our numerical model. The experimental samples exhibited the same fragmentation phenomenon: after more than 200 hours of thermal annealing, they became so fragile that a simple vibration could break them into pieces. In order to characterize this fragmentation process, we performed a

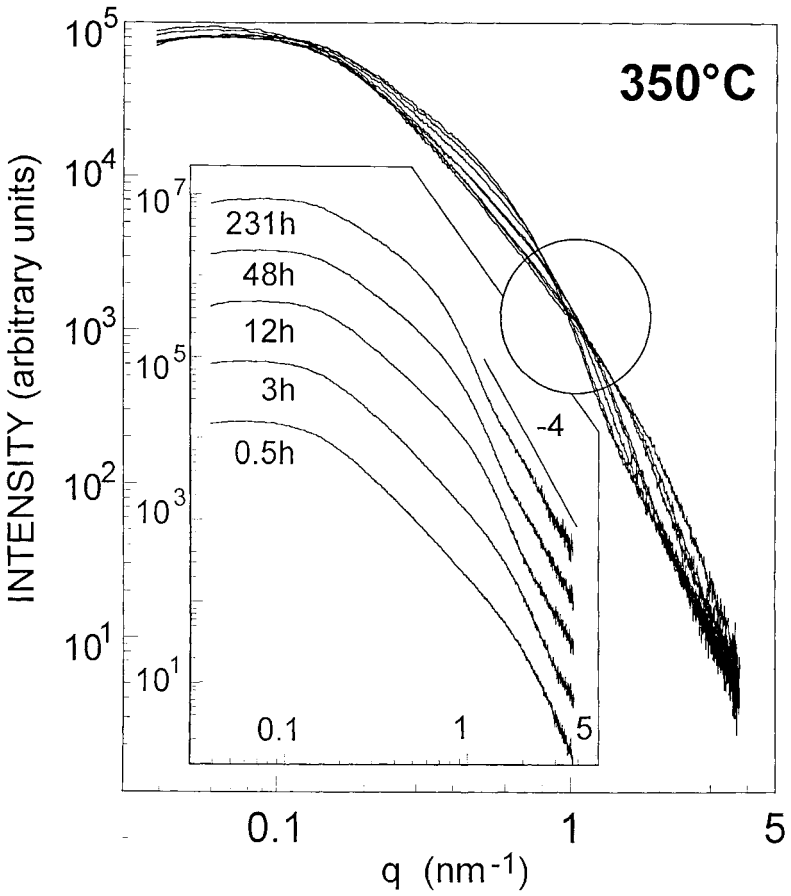

(a)

Figure 1. (a) Experimental SAXS intensity ($I(q)$ in arbitrary units) as a function of q (in nm^{-1}) for different durations of surface diffusion annealing. A circle has been drawn around the crossover region. The inset shows the curves offset for clarity. (b) Numerical small-angle scattering intensity ($I(q)$ in arbitrary units), for three different Monte Carlo time steps, as a function of q (in arbitrary units). The solid line represents $I(q)$ for the initial stage of thermal annealing, the dotted line shows the second stage of annealing and the long-dashed line shows the almost-final stage of annealing. A box has been drawn around the crossover region.

quantization of the size of the fragments. Figure 3 presents the size distribution of the particles in the sample for the initial stage and for the almost-final stage of annealing. The number of particles which have a size 2 is very important in the initial stage: this results from the DLCA aggregation computation for which we have used elementary particles with an edge length of 2. Then for the very final stage, this number of particles of size 2 would be near zero as would be the number of single subparticles, but, as we did not compute the process until the very end (equilibrium), small particles remain.

One has to remark that the number of particles which have a size 6 is almost constant. In view of this, we carried out an averaging over the size of all particles for the final stage and we found a mean size equal to 6.64. The same calculation was done for the initial stage and the mean size for particles was found to be equal to 2.39.

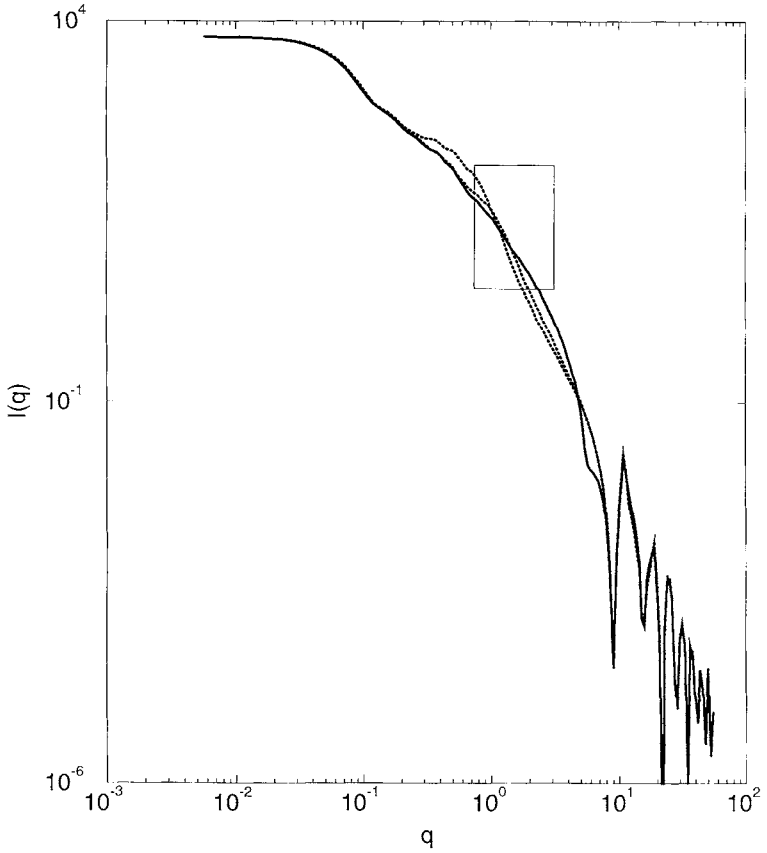

(b)

Figure 1. (Continued)

5. Discussion

Surface diffusion is a local transportation of matter. The matter moves from the locations where the curvature gradient is large to the locations where the curvature gradient is small. From an experimental point of view, matter has a mean transportation length which is very small. Similarly, in our simulation model, matter (i.e. subparticles) moves from one site to its very nearest neighbours. So the modelling of the process respects the local character of surface diffusion.

Two previous numerical simulations of this sort of matter transport have been carried out. The first, by Irisawa *et al* [2], used a model very similar to ours. During thermal relaxation, they observed fragmentation on two-dimensional fractal aggregates. The second simulation was done by Thouy *et al* [1] by resolving the diffusion equation on the contour of two-dimensional fractal aggregates with respect to the mass conservation. This diffusion equation takes account of the local curvature and hence appears as

$$\frac{\partial z}{\partial t} = C\frac{\partial^2 K}{\partial s^2} \tag{9}$$

where K is the local curvature, z is the local transverse displacement, s is the curvilinear

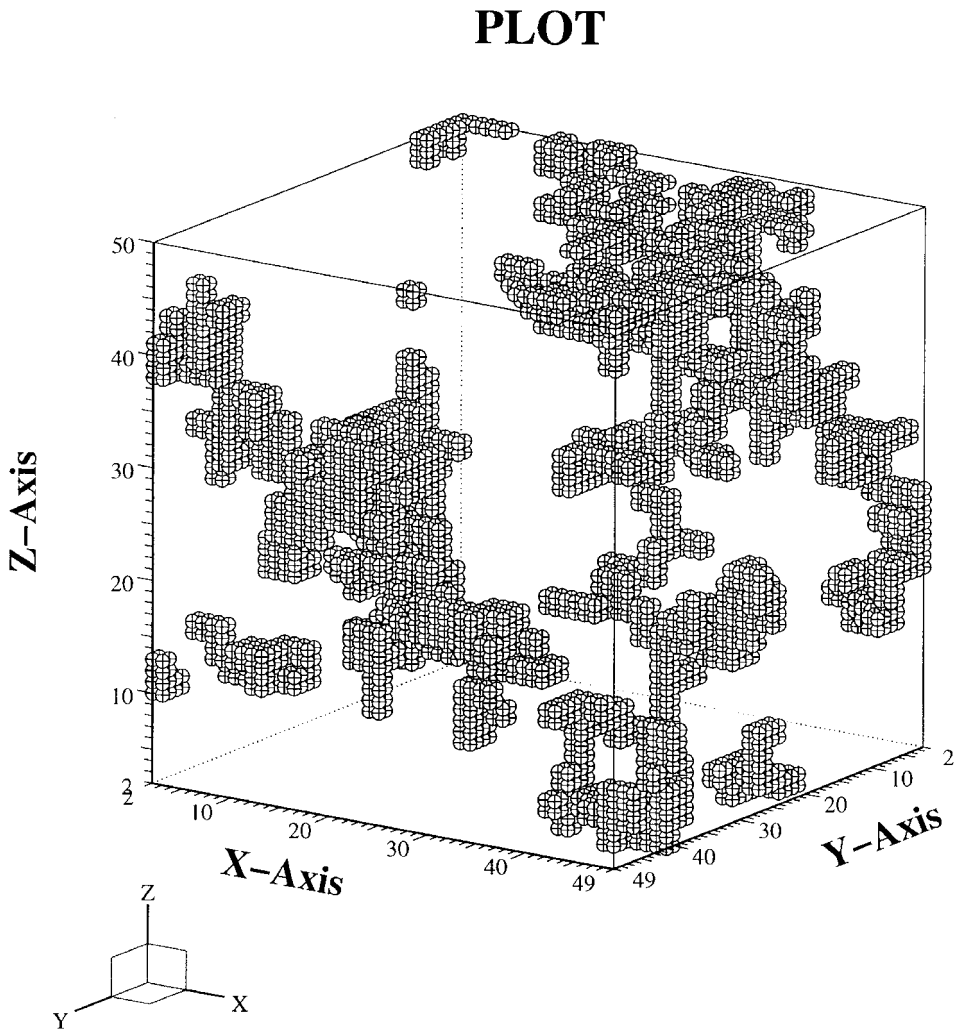

(a)

Figure 2. (a) Geometric representation of the internal structure of a DLCA aerogel before thermal annealing. This representation is 1/8 of the simulation box that we used in our calculations. (b) Geometric representation of the internal structure of a DLCA aerogel at the almost-final stage of surface diffusion annealing. Note the presence of several fragments.

coordinate and C is a constant which is given as

$$C = \frac{\ell_0^4}{(kT/D_s\gamma)} \tag{10}$$

where ℓ_0 is the typical size of the diffusing particle, k is the Boltzmann constant, D_s is the surface self-diffusion coefficient and γ is the surface tension (the last two being assumed to be isotropic). Equation (9) is commonly called the Mullins equation [13]. Thouy *et al* solved this equation on the contour of two-dimensional fractal aggregates of different sizes and for different fractal dimensions. Once again, they observed fragmentation.

Unlike these two previous studies, our modelling takes place in a three-dimensional space

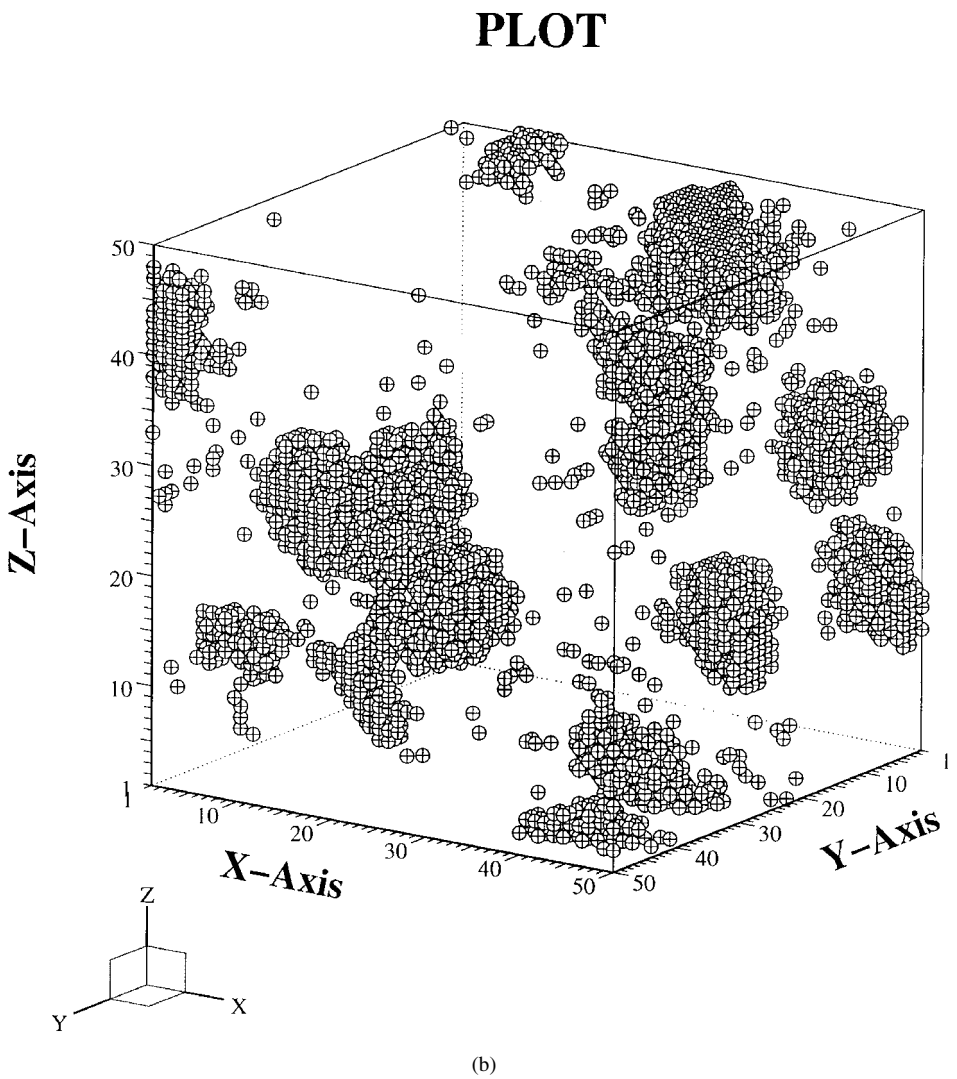

(b)

Figure 2. (Continued)

and deals with connected fractal aggregates in a cubic box. The dimensions of our simulation box (with periodic boundary conditions) remain constant throughout the simulation. So there is no shrinking in the size of the numerical aerogel. In the meantime, the low-q range of the small-angle scattering, which is sensitive to the size of the connected fractal clusters composing the aerogel, remains also almost constant during the different Monte Carlo steps.

The size of the particles in the numerical aerogel is calculated by counting the number of subparticles in the sample, which form a dense packing on the three-dimensional lattice. It is interesting to see that the numerical value of q for the crossover, on the calculated small-angle scattering intensity curve, is approximately equal to 1, so the characteristic length associated with this q is equal to 2π and the mean size of the particles or fragments as they are isolated fluctuates around 6.64 when there is no more evolution in the internal structure of the aerogel, i.e. for long durations of thermal annealing.

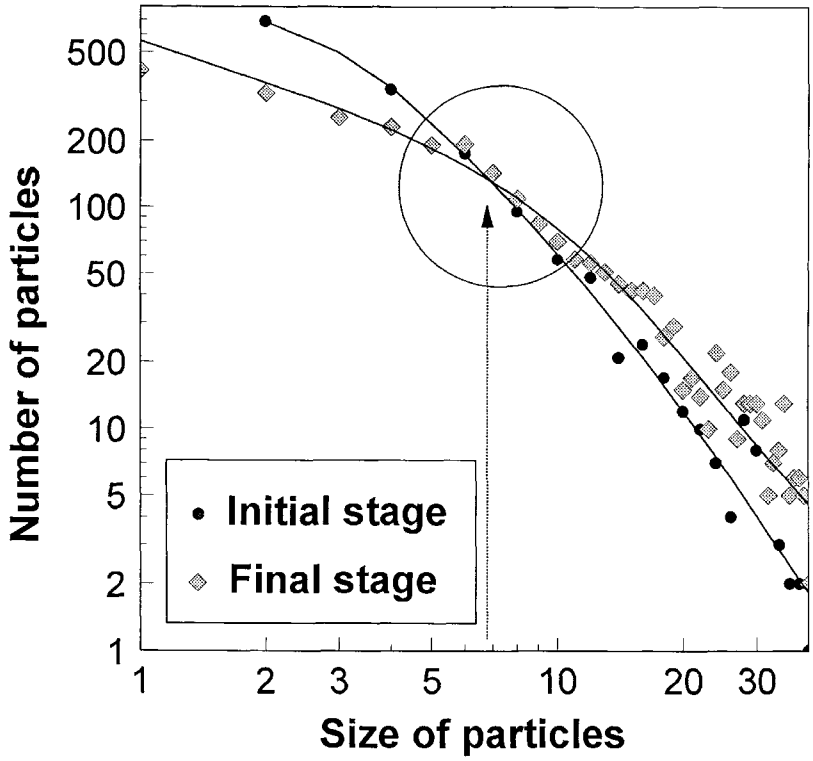

Figure 3. Numerical size distribution of the particles at the initial stage of the annealing and at the almost-final stage of the annealing. The numerical results are in units of a_0.

Moreover, the number of particles which have an edge length equal to 6 remains constant throughout the thermal relaxation: for the initial-stage size distribution and for the almost-final-stage size distribution, the number of fragments or particles with an edge length equal to 6 is roughly the same. This is, with the small-angle scattering curves, there is another way to characterize the crossover: the amount of matter on this length scale remains constant during thermal annealing. In the size distribution of fragments, one may see that the large fragments have a tendency to increase in size while the small fragments reduce in number.

The space distribution of matter is roughly the same for the almost-final stage of the thermal annealing as for the initial stage; this is due to the local nature of surface diffusion. As in reference [1], small-scale details of the internal structure tend to disappear. The inner surface is smoothed. The scattered intensity of the small-angle scattering curves decreases for q lower than $q_{crossover}$ as the quantity of matter on the length scale ℓ such that $2\pi/\ell < q_{crossover}$ decreases with time: the remaining particles attract all small subparticles in their neighbourhood; no more structures of length scale greater than ℓ remain. In fact, this length scale ℓ may be considered as the size of the particles or fragments at the final stage.

So, finally, for the small-angle scattering intensity curve, it is no longer appropriate to speak of a fractal slope. There is no longer a power law to express the curve modifications in the intermediate-q range. The general pattern of the space distribution of matter remains much the same but the local structure radically changes due to surface diffusion. All small-scale details are removed and all large-scale structures are contracted in isolated fragments.

All of this discussion is valid for the numerical part of our work but is also an explanation for the experimental results and phenomena.

Moreover, from an experimental point of view, the non-moving of the maximum-intensity-peak location means that the long-range correlations remain constant during annealing. The direct corollary is that there is no shrinking of the samples. On the other hand, the particle growth, obviously demonstrated both by SAXS and x-ray diffraction experiments, indicates that a matter flow has occurred. These two behaviours agree with the surface diffusion mechanism, which is well known to operate with or without a very low densification [3].

6. Conclusions

We have presented an experimental work on surface diffusion restructuring of zirconium oxide aerogels. The experimental results have been interpreted by way of a numerical model for the surface diffusion mobility as well as for the structure of zirconia aerogels. The particular features of the SAXS intensity curves have been explained by the computation of small-angle intensity curves based on the numerical results for the structure during thermal annealing. This allowed us to explain the crossover between SAXS intensity curves for different times by systematically studying the geometrical characteristics of the fragments which appear during the isothermal heat treatment. As a conclusion, we can say that there is a mean size of the fragments which corresponds to this crossover. Small-scale details are removed by surface diffusion but, at the length scale given by the crossover, the quantity of matter remains constant throughout the annealing experiments.

References

[1] Thouy R, Olivi-Tran N and Jullien R 1997 *Phys. Rev.* B **56** 5321
[2] Irisawa T, Uhawa M and Saito Y 1995 *Europhys. Lett.* **30** 139
[3] Wang J C 1990 *Metall. Trans.* A **21** 305
Wang J C 1991 *Concise Encyclopedia of Advanced Ceramic Materials* ed R J Brook (Oxford: Pergamon)
[4] Lecomte A, Blanchard F, Dauger A, Silva M C and Guinebetiere R 1998 *J. Non-Cryst. Solids* **225** 120
[5] Silva M C 1996 *PhD Thesis* Limoges University
[6] Jullien R and Botet R 1987 *Aggregation and Fractal Aggregates* (Singapore: World Scientific)
[7] Hasmy A, Anglaret E, Foret M, Pelous J and Jullien R 1994 *Phys. Rev.* B **50** 1305
[8] Guinier A and Fournet J 1955 *Small Angle Scattering of X-Rays* (New York: Wiley–Interscience)
[9] Feigin L and Svergun D 1987 *Structure Analysis by Small Angle X-Ray and Neutron Scattering* (New York: Plenum)
[10] Olivi-Tran N and Jullien R 1995 *Phys. Rev.* B **52** 258
[11] de la Rosa N, Gago-Duport L and Esquivas L 1995 *J. Non-Cryst. Solids* **192+193** 534
[12] Emmerling A, Gross J, Gerlach R, Goswin R, Reichenauer G, Fricke J and Haubold H-G 1990 *J. Non-Cryst. Solids* **125** 230
[13] Mullins W W 1957 *J. Appl. Phys.* **28** 333